

# A General Description of the Performance of Surface Plasmon Sensors Using a Transmission Line Resonant Circuit Model

Mengqi Shen and Michael G. Somekh

**Abstract**—We analyze the response of surface plasmon (SP) sensors using a transmission line model. We illustrate this analysis with particular reference to a layered structure in which plasmon hybridization occurs. By applying the appropriate resonant condition to the system, we derive a circuit model which predicts the responsivity of different modes. This gives new physical insight into the sensing process. We discuss how the change in the sample region may be modeled as a change in the reactance in the equivalent circuit and from this, it follows that a single parameter can determine the change in resonance position with reactance. This approach is used to predict the response of a generic sensor to binding of an analyte and the bulk change of refractive index. This parameter arises naturally from the circuit representation in a way not readily accessible with the transfer matrix approach. The parameters can be expressed in terms of the  $Q$  of a resonant circuit and confirms the intuition that a high  $Q$  is associated with poor responsivity, however, we demonstrate that there is another circuit parameter, the resistance at resonance, that can mitigate this effect, providing a route for optimization of the sensor properties.

**Index Terms**—Surface plasmons, multilayer design, biological sensing and sensors, transmission line model.

## I. INTRODUCTION

**S**URFACE plasmon resonance (SPR) is a powerful and well-established technique for measuring variations in refractive index. The SPR propagates between a metal and a dielectric and the SPR signal is very sensitive to changes in the dielectric, in terms of either variation of the bulk index or deposition of a thin layer on the metal surface [1].

Despite, the success of SPR there is always a need for even greater sensitivity especially when trying to detect molecules of small molecular weight and airborne contaminants at low concentrations. Moreover, the large incident angles in SPR measurements can be inconvenient especially in imaging applications. The main thrust of this paper is to recast the

surface wave sensing process in terms of a transmission line resonant circuit. In addition to unifying the description of the sensing process in a way compatible with electronic systems. We argue that this approach reveals some fundamental physical principles necessary for the optimization of sensor responsivity, that are not readily apparent with other descriptions. A transmission line model was considered in [2] to describe the Kretschmann configuration, however, no attempt was made to analyze the effect of sample deposition or examine the factors that lead to sensor responsivity.

We list some of the merits of the transmission line method (TLM) model that will be discussed in this paper.

- 1) The effect of binding of an analyte or refractive index change can be represented as a change in impedance.
- 2) The structure is built up layer by layer so the effect of each layer in terms of the change in impedance can be readily observed. This could also be done with the transfer matrix approach but TLM provides a much more simple and natural way to do this.
- 3) TLM represents the system as circuit parameters and provides a very simple way to solve the dispersion relation and the resonance position for the whole structure. This representation allows one to calculate the change in resonant  $k$ -vector directly without fitting to a reflectivity curve. Representing the sensor as a resonant circuit allows key physical properties of the sensing process to be elucidated.
- 4) The real and imaginary parts of the impedance can be analyzed separately as resistance and reactance, which determine the sharpness of response and the resonant position, respectively. This simplifies the calculation process and provides insight into the contribution of each circuit element.

We employ the KO structure (Figure. 1(a)) as an exemplar to explain this method as it supports both plasmonic and Fabry Perot (FP) modes and can represent these different modes in the same framework. This enables us to use the TLM to model a structure with rich behavior, moreover, it has the advantage of representing the conventional Kretschmann configuration as a limiting case. We discussed the KO structure in some detail in [3] where we showed that it had many desirable properties for sensing. One of the principal advantages being that the FP modes can give good responsivity, in some cases considerably better than the SP modes, at low angles of incidence. For bulk

Manuscript received May 27, 2019; accepted July 21, 2019. Date of publication August 5, 2019; date of current version November 13, 2019. The work of M. Shen was supported by Shenzhen city, for his Post-Doctoral Fellowship. The associate editor coordinating the review of this article and approving it for publication was Dr. Ying Zhang. (Corresponding author: Michael G. Somekh.)

M. Shen is with the Shenzhen Key Laboratory of Micro-Scale Optical Information Technology, Nanophotonics Research Centre, Shenzhen University, Shenzhen 518060, China (e-mail: shen.mengqi@szu.edu.cn).

M. G. Somekh is with the Shenzhen Key Laboratory of Micro-Scale Optical Information Technology, Nanophotonics Research Centre, Shenzhen University, Shenzhen 518060, China, and also with the Faculty of Engineering, University of Nottingham, Nottingham NG7 2RD, U.K. (e-mail: mike.somekh@szu.edu.cn).

Digital Object Identifier 10.1109/JSEN.2019.2933320

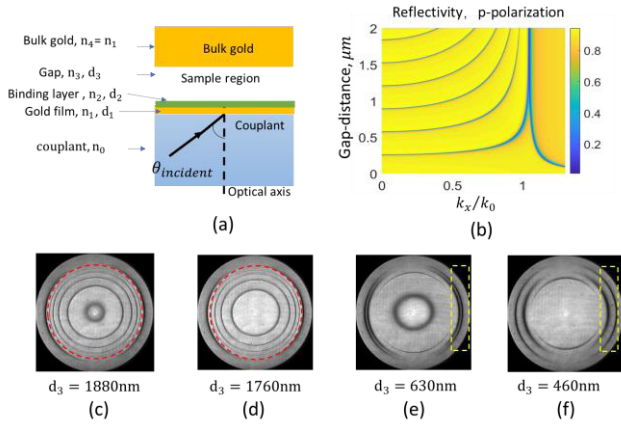


Fig. 1. (a) Schematic of the KO structure with a gap separation between bulk gold and Kretschmann structures; (b) variation of p-polarized reflectivity with the product of sine of the incident angle and the index of the couplant and gap distance for KO structure; (c) to (f) Experimental BFP distributions obtained with a 1.3 numerical aperture oil immersion objective for horizontal linear polarization at 633nm wavelength (c) Gap-distance=1880 nm; (d) Gap-distance=1760 nm; (e) Gap-distance=630 nm; (f) Gap-distance=460 nm. Modes within the red dashed circle, in (c) and (d) corresponding to the critical angle in air, are FP modes, modes within the yellow dashed box in (e) and (f) are hybridized SP modes.

refractive index sensing where low probe angles are beneficial the FP modes are very attractive compared to the SP mode.

We now summarize some of the properties of the KO structure to put our later discussions in context. The structure shown in Figure.1(a) is a hybrid structure combining features of the Otto configuration [4] and Kretschmann configuration [5] by placing bulk gold on top of conventional Kretschmann sensor. In our case, the separation between the gold surfaces was adjustable, since the bulk gold was mounted on a precision actuator. Figure.1(b) shows the p-polarized reflection intensity in response to the layer and bulk moves by a factor of 1.8 times and 10 times, respectively, compared to the SP modes, however, at the cost of wider dip transition. Each dip is also associated with a phase transition, which can also be used as a sensitive measure of the sensing process [6]. It is therefore possible to achieve high layer and bulk responsivity at smaller excitation angles in the KO structure.

We define the layer responsivity,  $R_l$ , of the sensor for specific values  $n_2$  and  $n_3$  as:

$$R_l = \frac{dn_0 \sin \theta_p}{dd_2} \quad (1)$$

where  $n_0$  is the refractive index of the coupling medium and  $\theta_p$  is the angle of the minimum of the dip (almost but not exactly equal to the resonance position [7]) and  $d_2$  is the thickness of the binding layer. And the bulk responsivity,  $R_b$ , of the sensor for specific values of  $n_3$  is defined as:

$$R_b = \frac{dn_0 \sin \theta_p}{dn_3} \quad (2)$$

It should be noted that throughout this paper we use the parameter  $k_x/k_0 (= n_0 \sin \theta)$  to denote the incident beam. Clearly, this value can be readily converted to an actual angle once the index of the coupling medium is known. For different resonance conditions this value is almost unchanged regardless of the value of  $n_0$ . Finally, it is important to point out the

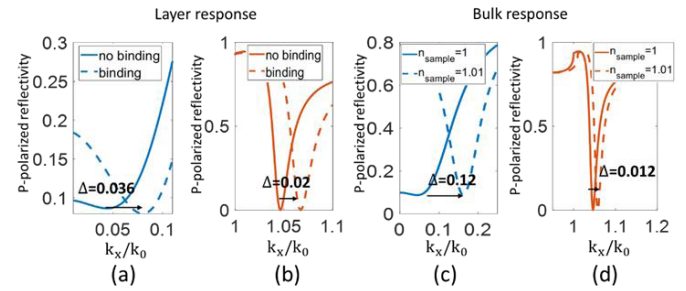


Fig. 2. (a) Layer response of 1<sup>st</sup> order FP mode in KO structure at  $d_3 = 576\text{nm}$ ; (b) layer response of SP mode in Kretschmann structure; (c) bulk response of 1<sup>st</sup> order FP mode in KO structure at  $d=576\text{nm}$ ; (d) bulk response of SP mode in Kretschmann structure.

Figure.2 compares the movement of the resonance position between the KO structure ( $n_0 = 1.52, \epsilon_1 = \epsilon_1 = \epsilon_{au} = -12.33 + 1.21i, n_2 = 1.4, n_3 = 1, d_3 = 576\text{nm}$ ) (blue color) and 50nm gold film based Kretschmann structure (red color) at 633nm wavelength with layer deposition and change of bulk refractive index, respectively. Figure.2(a) and (b) shows the movement of resonance position in response to 10nm BSA layer ( $n_2 = 1.4$ ) on top of gold film for KO structure and Kretschmann structure, respectively. Figure.2(c) and (d) compares the change of resonance position with refractive index in the sample region changing from 1 to 1.01 in the KO structure and Kretschmann structure, respectively. It can be observed that at 576nm gap-separation, 1<sup>st</sup> order FP mode is excited at  $k_x/k_0 = 0.04377$  in the KO structure. Solid lines and dashed lines denote the response before and after the change in the sample region, respectively. It shows that compared to the SP mode in the Kretschmann structure, the change of resonance position of the 1<sup>st</sup> order FP mode at 576nm gap separation in response to the layer and bulk moves by a factor of 1.8 times and 10 times, respectively, compared to the SP modes, however, at the cost of wider dip transition. Each dip is also associated with a phase transition, which can also be used as a sensitive measure of the sensing process [6]. It is therefore possible to achieve high layer and bulk responsivity at smaller excitation angles in the KO structure.

We define the layer responsivity,  $R_l$ , of the sensor for specific values  $n_2$  and  $n_3$  as:

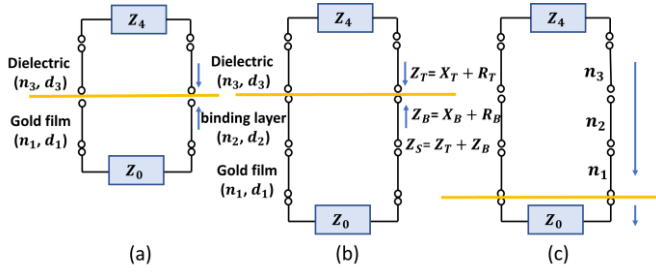


Fig. 3. (a) Shows the equivalent transmission line model of the structure for bulk change situation; (b) shows the equivalent transmission line model of the structure for binding situation; (c) denotes the reflectance. The yellow lines are the reference planes used in the analysis. The arrows in (a), (b) and (c) denote the direction required to project the impedance.

responsivity as determined by the movement of the dip is not the same as the sensitivity. The sharpness of the resonance affects the sensitivity, indeed the effect of the sharpness of the dip depends on the precise method of detection. This is discussed for different detection methods in [3].

## II. TRANSMISSION LINE MODEL

The physical basis of the performance of this structure is explained by its equivalent transmission line circuit. By employing this model, a KO structure is mapped to an equivalent RLC circuit. The approach to convert a structure into its equivalent transmission line model is introduced and a general explanation for the higher responsivity for this structure is given based on this model.

The equivalent transmission line model can be used to solve for different parameters of the system (e.g. reflection coefficient, resonance condition, Q factor) within the RLC circuit.

The principal stages in application of the transmission line model are described below. The differences between the use of the model to determine the reflection coefficient and the resonant conditions are discussed at the end.

Step 1: Decompose the target structure into component parts and view them as a number of interfaces connected by appropriate transmission regions. Figure.3 shows the gold film, the binding layer and the dielectric gap, which are represented as a transmission line with their specific length, the bulk gold and coupling medium are represented as  $Z_4$  and  $Z_0$ , respectively.

It is worth briefly elaborating on the physical meaning of each layer. In all cases medium 1 is the lower gold layer. For the Kretschmann configuration (Figure. 1(a)) layer  $n_3$  incorporates the effect of the binding and  $Z_4$  is the upper dielectric layer. In the last section we discuss the effect of inserting a dielectric between  $n_1$  and  $n_3$ , but this is not part of the usual Kretschmann configuration, so  $n_2$  is usually absent from the Kretschmann structures. For the KO configuration (Figure. 1(b)) the analyte is a binding layer  $n_2$  or a change in the bulk index  $n_3$ . The final impedance  $Z_4$  corresponds to bulk gold and is thus entirely different from the  $Z_4$  in the Kretschmann case.

Step 2: Select an interface as a reference plane, the choice of plane is a matter of convenience. The solutions of the

resonance positions and the corresponding Q factors are the same no matter which reference plane is chosen. The impedance can be transformed from one end to any interface based on the well-known relation for impedance transformation through a transmission line [8].

$$Z_{in} = Z_i \frac{Z_{ter} + Z_i \tanh(-jk_{zi}d_i)}{Z_i + Z_{ter} \tanh(-jk_{zi}d_i)} \quad (3)$$

$Z_{in}$  is the impedance seen after the terminating impedance,  $Z_{ter}$ , is the impedance propagated through the section of line with characteristic impedance  $Z_i$ ,  $d_i$  is the length of transmission region,  $k_{zi}$  is the wavevector along z-direction in the transmission region. The characteristic impedance for transverse electric (TE) and transverse magnetic (TM) waves propagating obliquely at an angle  $\theta$  are expressed as [9]:

$$Z_{TM} = \sqrt{\frac{\mu_0}{\epsilon}} \cos\theta, Z_{TE} = \sqrt{\frac{\mu_0}{\epsilon}} \frac{1}{\cos\theta} \quad (4)$$

In Figure.3(b), the impedances  $Z_T$  and  $Z_B$  are projected from top end and bottom end to the reference plane, respectively, in opposite directions.  $Z_T$  and  $Z_B$  corresponding to the top and bottom regions are complex values and can be represented as the sum of reactance (X) and resistance (R). The whole structure impedance  $Z_S$  is the summation of  $Z_T$  and  $Z_B$ .

Step 3: After the impedances are transferred from two sides to the reference plane either (i) the transverse resonance condition or (ii) the resonance condition (see below) is applied.

- (i) The condition for the transverse resonance condition is that the sum of the impedances is zero as shown in Eq. (5); the arrows in Figure.2 indicate the different propagation directions as discussed below [10].

$$\vec{Z}_T + \vec{Z}_B = 0 \quad (5)$$

By solving the transverse resonance condition, we obtain a complex solution of  $k$ -vector ( $k'_{sp} + ik''_{sp}$ ) that cancels both the reactance and resistance in the equivalent RLC circuit. The solution of  $k'_{sp} + ik''_{sp}$  is obtained when the sum of  $X_T$  and  $X_B$  is zero and the sum of  $R_T$  and  $R_B$  is also zero. This solution gives both the propagation constant and the attenuation of the excited wave.

- (ii) The resonance condition is useful when  $k_x$  is restricted to real values. This is satisfied when the reactance in the circuit are cancelled out, as shown in Eq (6).

$$\text{imag}(\vec{Z}_T + \vec{Z}_B) = 0 \text{ subject to } k_x \text{ being real.} \quad (6)$$

By solving for the resonance condition, a solution,  $k_{sp,o}$ , is obtained, which is relevant for the cases of the incident wave with a real angle, in other words, it is related to the actual measurement, where the system is excited with a propagating plane wave incident from the coupling medium. This solution makes the sum of  $X_T$  and  $X_B$  zero while the circuit still exhibits a residual resistance. The value of  $k'_{sp}$  obtained from transverse resonance condition and  $k_{sp,o}$  from the resonance condition are approximately the same when  $k'_{sp} \gg k''_{sp}$  (high Q factor). The Q factor is defined as the frequency-to-bandwidth ratio of the resonator, in our case,

it is modified as  $k_{sp}/\Delta k_x$ , and  $\Delta k_x$  is the full width half-power bandwidth where reactance is equal to resistance, so the  $\Delta k_x$  is  $2(dk_x/dX_s)R_s|_{k_x=k_{sp,o}}$ . This uses the fact that at the half power position the reactance is equal to the resistance. It also assumes that around the resonance region the variation in  $R_s$  is not significant; this assumption is valid as, in all cases, the variation was less than 1%. Therefore, we can define the Q factor around the resonance position,  $k_{sp,o}$ , as:

$$Q = \frac{k_{sp,o} \frac{dX_s}{dk_x}}{2R_s} \quad (7)$$

where  $X_s$  is the structure reactance,  $R_s$  is the structure resistance at the resonance position,  $X_s$  is zero. When the Q is high, the complex solution of  $(k'_{sp} + ik''_{sp})$  is close to the real axis with  $k'_{sp}$  very nearly equal to  $k_{sp,o}$ . Let us consider the Kretschmann structure with 50nm thick gold layer ( $\epsilon_{au} = -12.33 + 1.21i$ ) at 633nm wavelength, from Eq. 7 the Q factor is calculated as 60, and there is 0.038% difference between  $k'_{sp}$  and  $k_{sp,o}$ . When we increase the loss of the structure ( $\epsilon_{au} = -12.33 + 3.4i$ ) the Q factor is equal to 36, the error of  $k_{sp,o}$  increases then to 1%. The relative difference between  $k'_{sp}$  and  $k_{sp,o}$ , for all the cases discussed in the paper was always less than 1%. Although the discussion above has been focused on SP modes the same considerations are valid for the FP modes as confirmed in the experimental section later in the paper.

In the present paper, we explain the responsivity in terms of dip movement, Eq. (6) is employed in subsequent sections. Another advantage of using the TLM method to analyze the resonance position is that only the reactance (imaginary part) of the impedance needs to be considered for the high Q case which simplifies the calculation process.

The same dispersion relation is obtained regardless of which interface is chosen, however, it should be noted that  $k_z$  changes sign either side of the interface. This arises because the impedance is projected in different directions towards the interface [10], hence the direction of the arrows in Eq. (5) and Eq (6) and Figure. 3.

In this specific KO structure, we select the binding layer/air gap interface as the reference plane as shown in Figure.3(b).  $Z_T$  in Figure.3 (a) is therefore the top impedance which includes the information of bulk gold and air gap.  $Z_B$  is the bottom impedance transferred from the coupling medium to the reference plane which contains coupling medium, gold film and the binding layer.

To use the transmission line method to calculate the reflection coefficient the impedance is projected to the yellow interface of Figure.3(b), calling this impedance,  $Z_a$ , we can then simply obtain the reflection coefficient from:

$$\rho = \frac{Z_0 - Z_a}{Z_0 + Z_a} \quad (8)$$

The curves presented in Figure.2 were obtained by employing the TLM and select the coupling medium/gold film as the reference plane as described in Figure.3(b). In fact, our code to calculate the reflectivity with TLM, while, of course, giving identical results, runs several times faster than the equivalent transmission matrix code, although in most cases when only

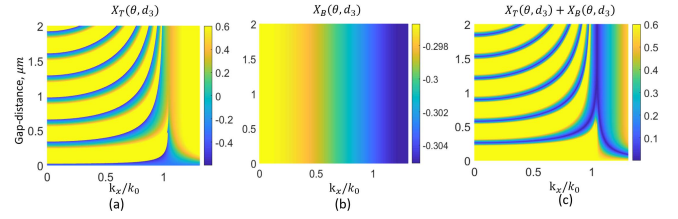


Fig. 4. (a) Variation of  $X_T$  with the product of the sine of incident angle and the index of the couplant and the gap-separation; (b) variation of  $X_B$  with the product of the sine of incident angle and the index of the couplant and the gap-separation; (c) shows the absolute value of the summation of (a) and (b).

a few parameters are changed, the run time is not significant for either method.

### III. EXPLANATION OF RESPONSIVITY

Sensors convert a change of the analyte to a measurable signal. In our case, the parameter we wish to detect is the change of reactance produced by the (i) binding layer or (ii) the change of bulk medium. According to the reference plane labeled in Figure.3(b), the binding layer produces an impedance change of  $\Delta X_B$ , while the change of bulk medium produces an impedance change of  $\Delta X_T$ . Both of these changes will disturb the current resonance condition and force the resonance condition to be satisfied in a new position. The difference of the resonance positions determines the signals we detect, which is related to the responsivity. It has been mentioned that for a fixed gap separation of the KO structure, multi-modes including FP modes and SP modes are obtained, and each mode has different responsivity. Therefore, for the same change of sample, the final responsivity is determined by two factors: (i) the change of  $k_x$  in response to a certain change of impedance; (ii) the relation between the impedance change and the incident angle for a specific change in sample region,  $\Delta X_T(\theta)$  or  $\Delta X_B(\theta)$ . In this section, the effect of the bulk dielectric layer will be discussed first and the two factors that decide the responsivity will be introduced.

#### A. Effect of Dielectric Layer Thickness

The modes produced in the KO structure have been explained using the resonance conditions in waveguide structure [11] and Maxwell's equations [12]. Here we explain these modes from the viewpoint of impedance and the corresponding RLC circuit. As shown in Figure. 3(a), the reference line at the binding layer/ dielectric gap separates the structure into  $Z_T$  and  $Z_B$ , respectively. The variation of  $X_T$  and  $X_B$  with different gap-separation at different angles are presented in fig. 4 (a) and (b), respectively. It can be seen in Figure.4 (b) that  $X_B$  decreases with increasing incident angle, since the air gap is not included in the bottom impedance, there is no change along the vertical direction. Figure. 4(a) shows the variation of  $X_T$ , in order to observe the positions that are close to the resonance conditions, the large values in this figure are saturated to a fixed value for clarity. We can see that below the critical angle the profile of  $X_T$  oscillates with changes in the gap-distance with a period given by  $\lambda/(2 \cos \theta)$ , where  $\theta$  denotes the wave propagation wave in the gap.

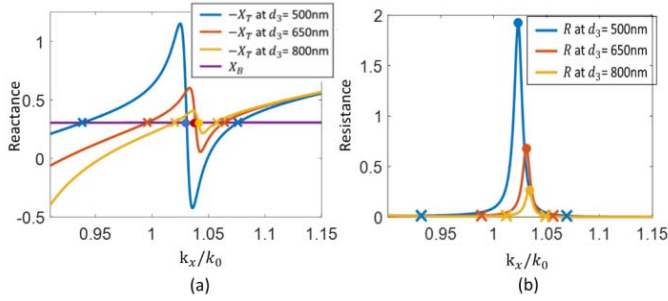


Fig. 5. (a) The variation of  $-X_T$  with various incident angles at  $d_3$  equal to 500nm (blue), 650nm (red) and 800nm (yellow), respectively, the purple line shows  $X_B$  and the intersections labeled as crosses between the  $X_B$  and  $-X_T$  are anti-symmetric modes and symmetric modes, respectively. The intersections labeled with circles do not manifest themselves in the reflection coefficient curve; (b) Variations of resistance with incident  $k$ -vector, showing a peak at the anti-resonance position.

Figure.4(c) shows the absolute value of the summation of Figure.4(a) and (b), and the positions with value equal to zero satisfy the resonance condition in Eq. (5).

Figure. 5 shows the variation of the top reactance  $-X_T$  at  $d_3$  equal to 500nm (blue), 650nm (red) and 800nm (yellow), respectively. The purple color describes the  $X_B$  and the intersections labeled as crosses between the  $X_B$  and  $-X_T$  are anti-symmetric modes and symmetric modes, respectively. The intersections labeled with circles are anti-resonance positions [13], these intersections do not manifest themselves in the reflection coefficient curve as this point does not represent a true mode. Since the transverse resonance position represents the  $k$ -vector of a true mode, the resonance condition must lie close to this value to excite the particular mode. This is satisfied only when the  $Q$  is high, this is not the case for the anti-resonant position as we can see there is a sharp peak (Figure. 5(b)) in the resistance, so satisfying the resonance condition of Eq. 6 does not mean that one is close to the transverse resonance position corresponding to a modal solution. Fig. 5a clearly shows the effect of hybridization and gives a clear graphical picture of the increased mode splitting with decreasing values of gap separation,  $d_3$ .

### B. The Change of $k_x$ in Response to a Change of Impedance

The sensor converts the change of sample to a measurable signal. The parameter we wish to detect is either the change of top impedance due to the change of refractive index in the gap,  $\Delta X_T$ , or the change of bottom impedance due to the change of the binding layer,  $\Delta X_B$ . From Figure.6 we can see that the whole structure reactance is displaced when a change of sample occurs, the solid line shows the relation between  $k_x$  and  $X_S$  at excitation position  $k_x = 2.27 \times 10^6$  before the change in sample region, is the corresponding line after deposition of the binding layer ( $n_2 = 1.4, d_2 = 10 \text{ nm}$ ) on the gold film. Over the range of  $k$ -vectors where the changes take place these two lines can be regarded as parallel, although this is not so over the very large range shown for illustrative purposes in Figure.6. The system responds by finding the new zero for the sum of the reactances, so  $k_{sp}$  must change to re-establish this condition. Since the two lines are almost parallel the change in impedance is provided by the gradient of

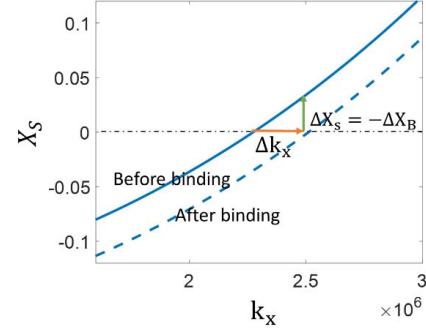


Fig. 6. The relation between  $k_x$  and  $X_S$  when resonance condition ( $X_S = 0$ ) satisfied at  $k_x = 2.27 \times 10^6$  before binding (blue solid), dashed line represents the relation after binding. The change of  $X_S$  due to binding must be compensated by a change,  $\Delta k_x$ .

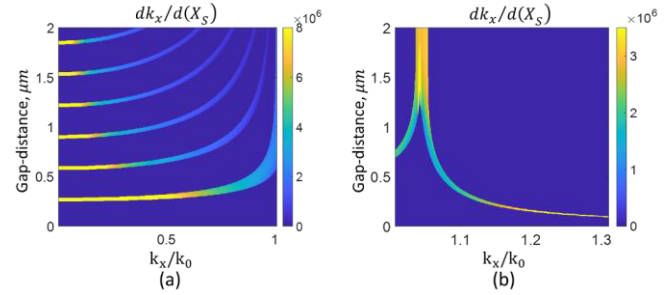


Fig. 7. (a) The gradient of  $k_x$  with respect to  $X_S$  at specific incident angles for various gap-separations for FP modes below the critical angle; (b) the gradient of  $k_x$  with respect to  $X_S$  at specific incident angles for various gap-separations for SP modes. Note the difference in scale between (a) and (b).

$X_S$  at the original resonance position. With this consideration, we can see that the change of dip position due to the change in sample region can be expressed as

$$\frac{dk_{sp}}{dX_T(\text{or } X_B)} = - \left. \frac{dk_x}{d(X_S)} \right|_{k_x=k_{sp,o}} \quad (9)$$

where  $k_x$  represents the real part of the incident wave number,  $X_S$  is the whole structure impedance which is the sum of  $X_T$  and  $X_B$ . Clearly, different gap-separations in the KO structure at different incident angles give different gradients, which means that a specific change of impedance in sample region changes the resonance position in proportion to that gradient. The value of  $dk_x/dX_S$  can be thought of as a key figure of merit of the sensor system indicating the resonance change due to a variation in sample region. It should be noted that the reciprocal of the  $dk_x/dX_S$  is proportional to the Q factor at resonance in Eq (7) which will be considered in more detail in the discussion.

The variation of the RHS term in Eq. (9) as a function of  $k_x$  and  $d_3$  shown in Figure.7 (a) and (b) for FP modes below the critical angles and SP modes above the critical angles, respectively. In our cases, the differential values around the resonance positions are shown and some very large values are saturated to make the data over the range clear. It can be observed in Figure.7 (a) that for the FP modes, at a specific gap-separation, the differential value decreases with the increase of incident angle and also decreases with gap-separation. The gradient also decreases for the anti-symmetric

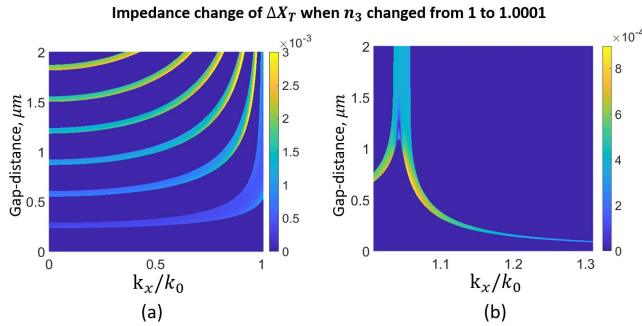


Fig. 8. Impedance change due to a change in bulk index. (a) the impedance changes of  $X_T$  at specific incident angles and various gap-separations for FP modes; (b) the impedance changes of  $X_T$  at specific incident angles and various gap-separations for SP modes thickness of gold.

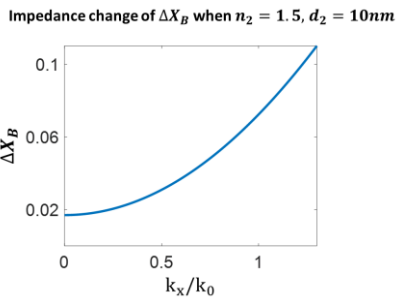


Fig. 9. Impedance change with layer deposition. The impedance changes of  $X_B$  at different incident angles. Note that this impedance change is continuous across the critical angle.

plasmon mode equaling the value of the zero order FP at the critical angle (the different coloring of these points simply arises from the different scales).

### C. Impedance Change Due to Change in the Analyte

The previous section discussed the response of the sensor from the point of view of a resonator responding to a change in load impedance. One further factor is required to complete the story on responsivity, namely the change in impedance generated by a physical change in the analyte. This variation is a function of  $k_x$  and also the surrounding structure. Two cases are considered in this section: (i) bulk change of the refractive index change in the gap; (b) deposition of a thin dielectric layer on the gold film. For the bulk case the change in reactance when  $n_3$  changed from 1 to 1.0001 at various incident angles and gap separations is shown in fig. 8(a) and (b) for FP modes and SP modes, respectively. We can see that in Figure.8(a), the change of impedance of FP modes increase with increasing incident angle and the gap-separation. Above the critical angle in fig.8 (b), the change of impedance due to the bulk index change decreases of both of the hybridized SP modes decreases as the gap separation until they merge to the position of the conventional SP mode. Fig.9 shows the reactance change of  $X_B$  due to a binding layer ( $n_2 = 1.5, d_2 = 10nm$ ), we can see that the change of reactance due to a layer binding on the gold film increases with the increase of incident angle. Since the bottom layer

TABLE I  
THE BFP DISTRIBUTIONS OF THE KO STRUCTURE AT  
 $D_3 = 900nm$  SY: SYMMETRIC MODE

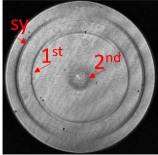
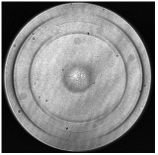
	Before binding	After binding
Experimental BFP distributions		
Mode	sy	1.054
positions	1 <sup>st</sup>	0.7996
( $k_x/k_0$ )	2 <sup>nd</sup>	0.1351
		0.1525

TABLE II  
COMPARISON THE CALCULATION OF THE CHANGE OF  
RESONANCE POSITION BETWEEN TRANSMISSION  
LINE PREDICTION AND FRESNEL EQUATIONS

Mode number	Factor 1: $dk_{sp}/dX_S$	Factor 2: $\Delta X_B$	Product of factor 1 and 2 (Eq. 10)	$\Delta k_x$ (experimental)
sy	$2.24 \times 10^6$	0.1054	$2.36 \times 10^5$	$2.58 \times 10^5$
1 <sup>st</sup>	$1.187 \times 10^6$	0.0702	$0.83 \times 10^5$	$0.804 \times 10^5$
2 <sup>nd</sup>	$8.14 \times 10^6$	0.023	$1.8 \times 10^5$	$1.68 \times 10^5$

is not associated with the gap separation, for a specific layer these changes are a function of incident angle only.

The change of resonance condition is obtained from the product of the terms in Figure.7 and the corresponding curve in fig.8 and fig.9 for bulk change and layer change, respectively. This is discussed explicitly in the following section with reference to experimental measurements.

## IV. COMPARISON WITH EXPERIMENTAL RESULTS

We now present experimental results to demonstrate this method. In table 1, the experimental BFP images are captured using an objective lens with NA=1.3 at 633nm wavelength when the dielectric gap-separation in KO structure is 900nm. It can be seen that the 2<sup>nd</sup> order FP mode, 1<sup>st</sup> order FP mode and the symmetric SP mode can be observed clearly, while the anti-symmetric mode is weak at this gap-separation. The corresponding excitation position in the unit of  $k_x/k_0$  for symmetric SP modes, 1<sup>st</sup> FP mode and 2<sup>nd</sup> FP mode are 1.054, 0.7996 and 0.135, respectively, before binding. When a 15nm thick BSA layer ( $n_2 = 1.4$ ) is deposited on the gold film, the position of each mode changes to 1.08, 0.8077 and 0.1525, respectively. Table 2 shows how this responsivity arises from the terms in Eq. 5. Based on the transmission line model, the differential factor for the modes presented in Table. 2. The change of bottom impedance,  $\Delta X_B$ , due to the 15nm thick BSA is listed in the third column in Table. 2 for the different modes. The fourth column in Table. 2 lists

the predicted change of resonance according to the product of the two factors in transmission line model, while the data in the last column is the measured value obtained from the experimental BFP data. The deviation arises from uncertainty in the parameters and also because Eq. (8) is effectively a first order perturbation analysis [14].

The factors in Table. 2 can therefore be seen to give very good agreement with the experimental results. For the experimentally measured layer sensitivity the symmetric plasmon gives the best responsivity because the evanescent wave interacts with the layer. For bulk sensitivity the equivalent parameters are for  $\Delta X_T$  are: sy:  $6.15 \times 10^{-4}$ , 1<sup>st</sup> order FP:  $1.08 \times 10^{-3}$  and 2<sup>nd</sup> order FP:  $1.03 \times 10^{-3}$ . Multiplying this impedance change by factor 1 from Table 2 gives sensitivities in the following ratios: sy:1<sup>st</sup>:2<sup>nd</sup> = 1:0.92:6.09. In this case the FP modes can have similar or better responsivity than SP for bulk index changes, partly because the propagating mode can penetrate the whole medium. For layer sensitivity the SP is generally more responsive.

## V. DISCUSSION

From the considerations of section 2, we can say that the responsivity of the system for an impedance change due to analyte is given by:

$$\frac{dk_x}{dX_s} = \frac{k_{sp,o}}{2QR_s} = A \quad (10)$$

Then the total responsivities of Eq.1 and Eq.2 are given by  $R_l = \frac{1}{k_0} A \frac{dX_s}{dd_2}$  and similarly  $R_b = \frac{1}{k_0} A \frac{dX_s}{dm_3}$ . From the results of section 4 we can see the interplay of these factors. Comparing the results of Table. 2 we see that the  $A$  value for the 2<sup>nd</sup> FP mode is extremely high, but for layered samples this is limited by the fact the reactance change is small at close to normal incidence, the symmetric plasmon mode despite a much smaller value of  $A$  still has more overall sensitivity due to the greater change of reactance. On the other hand, for bulk index responsivity the 2<sup>nd</sup> order FP mode benefits from both a larger value of  $A$  as well as the impedance change. The small angle of incidence of this mode means construction of the sensor is more convenient.

Examining Eq. 10 reveals an interesting and general trade-off. If we want a sensor with good responsivity operating at low incident angle then the value of the denominator must be small to compensate. This implies a very low value of  $Q$ , so that if we want good responsivity at low incident angles we need to accept that the response will be rather broad, which can limit the ultimate sensitivity of the sensor as discussed in [7].

It is worth discussing the form of the denominator in more detail. The responsivity is inversely proportional to the  $Q$  as we might expect. It is common knowledge in microwave engineering that the resonant frequency of a high  $Q$  cavity changes less to an external load compared to a low  $Q$  cavity. Eq. 10 tells us that the responsivity is also inversely proportional to the resistance, therefore, a high  $Q$  does not necessarily entail a poor responsivity if the value of  $R_s$  can be sufficiently low. This is not just an abstract notion as we can readily devise structures that illustrate this point. Consider Figure.10 which

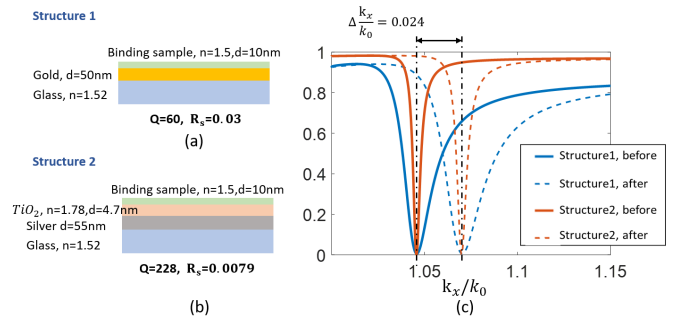


Fig. 10. (a) Schematic of Kretschmann structure; (b) schematic of silver based structure with a 4.7nm thick  $TiO_2$  layer deposit on the silver film; (c) comparison between structure 1 and structure 2 in terms of dip movement.

shows the usual Kretschmann configuration with a gold layer (structure 1) and a silver layer with high index layer deposited on it (structure 2). The resonant value for bare silver is somewhat less than gold, however, deposition of a dielectric  $TiO_2$  layer of thickness 4.7nm makes the resonant angle for both systems the same,  $k_{sp}/k_0 = 1.046$ . This means that  $k_x$  is the same, interestingly, we found that in Figure.10 (c) the movement of the resonant position in response to the same binding sample ( $n=1.5$ ,  $d=10nm$ ) for these two structures is almost identical, this means the value of  $A$  for each structure is the same. For structure 1 the calculated value of  $Q=60$  and the resistance around resonance the transition is 0.03, for structure 2, at resonance position,  $Q$  is 228 and resistance is 0.0079, the product of  $Q$  and  $R_s$  are the same for these two structures which ensures that they have the same responsivity (since  $k_x$  is also the same). This is demonstrated in Figure .10(c), the blue and red colors denote the data for structure 1 and structure 2, respectively, the solid line and dashed line show the data before binding and after binding. The higher  $Q$  factor in structure 2 is responsible for the narrower dip shape. We can therefore see that a high  $Q$  and small  $QR_s$  product are fundamental and slightly conflicting properties required to produce an ideal surface wave sensor. Clearly, the only way to satisfy both of these conditions is to ensure that the value of  $R_s$  is low.

## VI. SUMMARY

The present paper has given a new perspective on the performance parameters associated with sensors. The system is analyzed with a transmission line model and its associated equivalent circuit. The transmission line model provides a simple approach to the solution to the resonance condition. Moreover, the transmission line representation shows that the change in the sample region may be regarded as a change in reactance, so that for a given change in reactance, the responsivity of the system can be contained in a single parameter,  $-dk_x/dX_s$ , derived from the equivalent circuit. The model has demonstrated two important general properties of sensors that have not, to our knowledge, been hitherto explicitly stated, firstly the responsivity to a reactance change decreases with the resonant angle and secondly that the key parameter determining the responsivity is the inverse product the  $Q$  and the circuit resistance  $R_s$ , which can be interpreted as

proportional to the reciprocal the stored energy in the resonant circuit. The transmission line representation may also be used to model dielectric structures where there is no dip in the reflection coefficient, since the conditions for resonance and transverse resonance are still represented by the circuits of Figure.4. In this case, the resonance will be identified by the phase of the reflection coefficient. This analysis has enabled us to make general observations about the performance of sensor systems, which we believe can provide a valuable method to design new sensor systems in an efficient and physically intuitive manner.

## REFERENCES

- [1] P. Englebienne, A. Van Hoonacker, and M. Verhas, "Surface plasmon resonance: Principles, methods and applications in biomedical sciences," *Spectroscopy*, vol. 17, nos. 2–3, pp. 255–273, 2003.
- [2] A. Tarlis, J. Sarma, and F. Causa, "Transmission line circuit representation of surface plasmon waves," *Proc. SPIE*, vol. 6370, Oct. 2006, Art. no. 637017.
- [3] M. Shen, S. Learkthanakhachon, S. Pechprasarn, Y. Zhang, and M. G. Somekh, "Adjustable microscopic measurement of nanogap waveguide and plasmonic structures," *Appl. Opt.*, vol. 57, no. 13, pp. 3453–3462, May 2018.
- [4] A. Otto, "Excitation of nonradiative surface plasma waves in silver by the method of frustrated total reflection," *Zeitschrift für Physik A Hadrons and Nuclei*, vol. 214, no. 4, pp. 398–410, Aug. 1968.
- [5] E. Kretschmann and H. Raether, "Notizen: Radiative decay of non radiative surface plasmons excited by light," *Zeitschrift für Naturforschung*, vol. 23, no. 12, pp. 2135–2136, Dec. 1968.
- [6] Y. H. Huang, H. P. Ho, S. K. Kong, and A. V. Kabashin, "Phase-sensitive surface plasmon resonance biosensors: Methodology, instrumentation and applications," *Annalen der Physik*, vol. 524, no. 11, pp. 637–662, Nov. 2012.
- [7] A. V. Kabashin, S. Patskovsky, and A. N. Grigorenko, "Phase and amplitude sensitivities in surface plasmon resonance bio and chemical sensing," *Opt. Express*, vol. 17, no. 23, pp. 21191–21204, Nov. 2009.
- [8] U. A. Bakshi and A. V. Bakshi, *Transmission Lines and Waveguides*. Pune, Maharashtra: Technical Publication, 2009.
- [9] A. Polemi and K. L. Shuford, "Transmission line equivalent circuit model applied to a plasmonic grating nanosurface for light trapping," *Opt. Express*, vol. 20, no. S1, pp. A141–A156, Jan. 2011.
- [10] B. D. Bates and G. W. Staines, "Transverse resonance analysis technique for microwave and millimetre-wave circuits," DSTO Electron. Surveill. Res. Lab., Salisbury, SA, Australia, Tech. Rep. ADA299143, 1995.
- [11] P. Yeh, *Optical Waves in Layered Media*. Hoboken, NJ, USA: Wiley, 1998.
- [12] H. T. M. C. M. Baltar, K. Drozdowicz-Tomsia, and E. M. Goldys, "Propagating surface plasmons and dispersion relations for nanoscale multilayer metallic-dielectric films," in *Plasmonics-Principles and Applications*. Rijeka, Croatia: InTech, 2012, pp. 135–156.
- [13] A. F. McKinley, T. P. White, I. S. Maksymov, and K. R. Catchpole, "The analytical basis for the resonances and anti-resonances of loop antennas and meta-material ring resonators," *J. Appl. Phys.*, vol. 112, no. 9, 2012, Art. no. 094911.
- [14] T. Kato, *Perturbation Theory for Linear Operators*. Berlin, Germany: Springer, 1995.



**Mengqi Shen** received the Ph.D. degree from the University of Nottingham in 2018.

After a period of working as a Research Assistant with the Hong Kong Polytechnic University, she joined Shenzhen University as a Post-Doctoral Researcher. Her research interests include imaging, sensors, measurement, and detectors.



**Michael G. Somekh** received the first degree in metallurgy and science of materials from Oxford University and the Ph.D. degree in microwave electronics from Lancaster University, U.K. After research fellowships at Oxford University, his first academic position was with University College London. He then joined the University of Nottingham, Nottingham, U.K., where he founded the Applied Optics Group. After a period working in Hong Kong, he joined Shenzhen University as Distinguished Professor and also holds a part-time position with Nottingham University as a Professor of Optical Engineering.

He is a Fellow of the Institute of Physics and was elected Fellow of the Royal Academy of Engineering (the U.K. National Engineering Academy) in 2012 in recognition of his interdisciplinary work. His research interests include imaging, sensors, and ultrasonics.